

## Journal Pre-proof

Error-informed parallel adaptive Kriging method for time-dependent reliability analysis

Zhuo Hu, Chao Dang, Da Wang, Michael Beer, Lei Wang

PII: S0951-8320(25)00395-3  
DOI: <https://doi.org/10.1016/j.ress.2025.111194>  
Reference: RESS 111194  
To appear in: *Reliability Engineering and System Safety*



Please cite this article as: Z. Hu, C. Dang, D. Wang et al., Error-informed parallel adaptive Kriging method for time-dependent reliability analysis. *Reliability Engineering and System Safety* (2025), doi: <https://doi.org/10.1016/j.ress.2025.111194>.

This is a PDF file of an article that has undergone enhancements after acceptance, such as the addition of a cover page and metadata, and formatting for readability, but it is not yet the definitive version of record. This version will undergo additional copyediting, typesetting and review before it is published in its final form, but we are providing this version to give early visibility of the article. Please note that, during the production process, errors may be discovered which could affect the content, and all legal disclaimers that apply to the journal pertain.

© 2025 Published by Elsevier Ltd.

# Error-informed parallel adaptive Kriging method for time-dependent reliability analysis

Zhuo Hu<sup>a</sup>, Chao Dang<sup>b</sup>, Da Wang<sup>a</sup>, Michael Beer<sup>c,d,e</sup>, Lei Wang<sup>f,\*</sup>

<sup>a</sup>School of Civil Engineering, Central South University of Forestry & Technology, Changsha 410004, PR China

<sup>b</sup>Chair for Reliability Engineering, TU Dortmund University, Leonhard-Euler-Str. 5, Dortmund 44227, Germany

<sup>c</sup>Institute for Risk and Reliability, Leibniz University Hannover, Callinstr. 34, Hannover 30167, Germany

<sup>d</sup>Department of Civil and Environmental Engineering, University of Liverpool, Liverpool L69 3GH, United Kingdom

<sup>e</sup>International Joint Research Center for Resilient Infrastructure & International Joint Research Center for Engineering Reliability and Stochastic Mechanics, Tongji University, Shanghai 200092, PR China

<sup>f</sup>School of Civil Engineering, Changsha University of Science & Technology, Changsha 410114, PR China

## Abstract

Active learning single-loop Kriging methods have gained significant attention for time-dependent reliability analysis. However, it still remains a challenge to estimate the time-dependent failure probability efficiently and accurately in practical engineering problems. This study proposes a new method, called ‘Error-informed Parallel Adaptive Kriging’ (EPAK) for efficient time-dependent reliability analysis. First, a sequential variance-amplified importance sampling technique is developed to estimate the time-dependent failure probability based on the trained global response Kriging model of the true performance function. Then, the maximum relative error of the time-dependent failure probability is derived to facilitate the construction of stopping criterion. Finally, a parallel sampling strategy is proposed through combining the relative error contribution and an influence function, which enables parallel computing and reduces the unnecessary limit state function evaluations caused by excessive clustering. The superior performance of the proposed method is validated through several examples. Numerical results demonstrate that the method can accurately estimate the time-dependent failure probability with higher efficiency than several compared methods.

**Keywords:** Time-dependent reliability analysis; Active learning; Kriging model; Importance sampling; Parallel computing; Estimation error

\*Corresponding authors

Email address: leiwang@csust.edu.cn (Lei Wang)

## 1. Introduction

Reliability analysis aims to assess the likelihood that a structural system or component will consistently perform the intended functions when considering multi-source uncertainties, such as material properties, applied loads, geometry, model uncertainty, and others [1]. The traditional time-invariant reliability analysis neglects the time-dependent factors and is limited to assessing the reliability at a specific time instant. Considering the fact that the performance of engineered component or systems usually degrades with the increase of service time, time-dependent reliability analysis (TRA) has drawn much attention in recent decades [2–4]. Incorporating the time dimension adds complexity to the problem, which makes the TRA more time-consuming than the time-invariant cases [5, 6]. The current TRA methods could be categorized into three following groups: (1) out-crossing rate methods; (2) composite limit state methods; (3) extreme value methods.

In the out-crossing rate methods, the time-dependent failure probability (TDFP) is approximated by integrating the instantaneous out-crossing rate over a specified time interval. The origin of this type of methods can be tracked into the 1940s when Rice introduced the famous Rice formula [7], laying the theoretical foundation for the development of the out-crossing rate methods for time-dependent reliability problems. The out-crossing rate methods can be further classified into the two following groups. The first group consists of the numerical methods, mainly based on the FORM or the method of moments. The representative methods include PHI2 [8], PHI2+ [9], and MPM2 [10], etc. The second is the analytical methods, including but not limited to [11–13]. Although the performance of the out-crossing rate methods have been improved in the last several decades [14, 15], the large computation cost and the inherent assumption still restrict the applicability of the out-crossing rate methods in TRA.

The composite limit state methods discretize the time-dependent limit state function (LSF) into a series of instantaneous LSFs, thereby transforming the time-dependent issue into a time-invariant one with the series system reliability concept [16]. Some studies use FORM to calculate the instantaneous reliability, including but not limited to [17–19]. These methods may produce inaccurate results when the LSF is highly nonlinear or contains multiple most probable points (MPPs). Simulation-based methods have also

been developed for TRA, e.g., subset simulation [20], line sampling [21] and importance sampling [22], etc. Despite better accuracy, the simulation-based methods still suffer from low efficiency in engineering practices.

The extreme value methods transform the time-dependent problem into a time-invariant one, and the TDFP is estimated by solving the extreme value distribution [23, 24]. Recent advancements in artificial intelligence have accelerated the application of machine learning in predicting the extreme value distribution, where adaptive surrogate models have gained significant attention for their effective balance between accuracy and efficiency [25–27]. The extreme response surrogate-based methods, as a type of double-loop methods, need to identify the extreme response in the inner loop and build a surrogate model for the extreme response in the outer loop [28]. The typical methods falling into this category include the parallel efficient global optimization [29], confidence-based adaptive extreme response surface method [30], importance sampling-based double-loop Kriging [31], mixed EGO method [32] and so forth. The double-loop methods may suffer from low accuracy due to the fact the accuracy of searching extreme time instant would influence the accuracy of surrogate model. Besides, this kind of method requires a large amount LSF evaluations for the problems with stochastic process with a long time interval. Instead of a double-loop scheme, a single-loop scheme involving constructing the global response surrogate models has been extensively investigated [33, 34]. Among the various kinds of surrogates, the Kriging model is particularly prominent for its capability to interpolate and provide a local measure of prediction uncertainty. In this regard, the most pioneering is the single-loop Kriging surrogate modeling (SILK) method [33]. Some other representative single-loop methods include variance reduction-guided adaptive Kriging (VARAK) method [35], real-time estimation error-guided active learning Kriging (REAL) method [36], single-loop Gaussian process regression based-active learning (SL-GPR-AL) method [37], and several others [38, 39]. In the aforementioned single-loop methods, the estimation of the TDFP is all based on Monte Carlo Simulation (MCS) and is computationally challenging for small failure probability problems. To solve this problem, several methods have been developed by combining the single-loop Kriging model with importance sampling technique [40, 41] and subset simulation [42–45], respectively. Recently, the first author and his co-authors [46] have

extended the Bayesian active learning originally developed for time-invariant reliability analysis [47–49] to the time-dependent counterpart, and proposed uncertainty-aware adaptive Bayesian inference combined with hyper-ring decomposition importance sampling for TRA. As mentioned in [36], the estimation error of TDFP is an important measure for assessing whether the TDFP is sufficiently accurate as the final result throughout the active learning process. To the best of authors’ knowledge, however, none of existing studies has attempt to quantify and reduce the estimation error of TDFP provided by Kriging model and importance sampling. Besides, these single-loop methods can only identify one point per iteration, hindering their availability of the parallel computing.

This study aims to propose a novel method termed ‘Error-informed Parallel Adaptive Kriging’ (EPAK) for efficient TRA. The primary contributions can be outlined as follows:

- The variance-amplified importance sampling (VAIS) proposed in [48] is adapted in a sequential way for estimating the small TDFPs. The resulting sequential VAIS can reduce the sample size and total computation time but also avoid the computer memory issue due to the one-shot Kriging prediction on the large amount of samples;
- The maximum relative error of the TDFP is derived under the combination of the single-loop Kriging model and VAIS. This allows the quantification of error in estimating TDFP, and facilitates the construction of an effective stopping criterion. In this study, the adaptive updating of Kriging model is terminated by judging the maximum relative error;
- A parallel sampling strategy is developed through combining the relative error contribution and an influence function that considers the correlation between the existing training points and the candidate points. This strategy can select multiple training points and overcome the problem of unnecessary LSF evaluations caused by excessive clustering.

The rest of this study is structured as follows. Section 2 introduces the estimation of TDFP based on Kriging and MCS. In section 3, the proposed EPAK method is presented in detail. Four examples are studied in Section 4 to validate the proposed method. Section 5 concludes the present study.

## 2. Background of time-dependent reliability analysis

In this section, we first give the definition of TDFP. The MCS-based TDFP estimation is then reviewed. The Kriging-based global response surrogate method is finally introduced.

### 2.1. Definition of time-dependent failure probability

The key to TRA is to calculate the failure probability (denoted as  $P_f(0, t_e)$ ) of a structural system or component within a predefined time interval  $[0, t_e]$ . A failure event is defined when the LSF is below zero at any time instant within  $[0, t_e]$ . Let  $g(\mathbf{X}, \mathbf{Y}(t), t)$  denote the LSF with an  $n$ -dimensional input vector of random variables  $\mathbf{X} = [X_1, X_2, \dots, X_n]$  and an  $m$ -dimensional input vector of stochastic processes  $\mathbf{Y}(t) = [Y_1(t), Y_2(t), \dots, Y_m(t)]$ , where  $t$  denotes the time parameter.

The TDFP  $P_f(0, t_e)$  is expressed as follows:

$$P_f(0, t_e) = \mathbb{P}\{g(\mathbf{X}, \mathbf{Y}(t), t) < 0, \exists t \in [0, t_e]\} \quad (1)$$

where  $\mathbb{P}$  denotes the operation of probability.

Assuming that the stochastic processes  $\mathbf{Y}(t)$  are represented by a function of the random variables  $\Xi$  and time parameter  $t$ , the TDFP can be expressed as an integral given by:

$$P_f(0, t_e) = \int_{\mathbb{R}^n} \int_{\mathbb{R}^\infty} I(\mathbf{x}, \mathbf{y}(\xi, t), t) f_{\mathbf{X}}(\mathbf{x}) f_{\Xi}(\xi) d\mathbf{x} d\xi \quad (2)$$

where  $I(\mathbf{x}, \mathbf{y}(\xi, t), t)$  is the time-dependent indicator function;  $\mathbf{x}$  and  $\xi$  are the realizations of  $\mathbf{X}$  and  $\Xi$ , respectively;  $f_{\mathbf{X}}(\mathbf{x})$  and  $f_{\Xi}(\xi)$  are the joint probability density functions (PDFs) of the random variables  $\mathbf{X}$  and  $\Xi$ , respectively;  $I(\mathbf{x}, \mathbf{y}(\xi, t), t)$  is written as:

$$I(\mathbf{x}, \mathbf{y}(\xi, t), t) = \begin{cases} 1, & g(\mathbf{x}, \mathbf{y}(\xi, t), t) < 0, \exists t \in [0, t_e] \\ 0, & \text{otherwise} \end{cases} \quad (3)$$

## 2.2. Discretization of stochastic processes

The stochastic processes  $\mathbf{Y}(t)$  are discretized into random variables for computation purposes. The commonly used expansion optimal linear estimation (EOLE) [50] is adopted in this study due to its high efficiency and accuracy. One should note that it is not straightforward to simulate non-Gaussian processes with EOLE method. For general stochastic processes, some advanced simulation methods can be used, e.g., [51, 52]. In this study, only Gaussian processes are considered for convenience.  $n_t$  time instants are employed to discretize the time interval  $[0, t_e]$ . Considering a Gaussian process  $Y(t)$  for the sake of illustration,  $Y(t)$  is written as:

$$Y(t) \approx \mu(t) + \sum_{i=1}^p \frac{\xi_i}{\sqrt{\lambda_i}} \phi_i^\top \boldsymbol{\rho}_Y(t) \quad (4)$$

where  $\mu(t)$  denotes the mean function;  $p$  denotes the number of dominated eigenvectors, which can be determined according to [8].  $\xi_i$  ( $i = 1, \dots, p$ ) denote the expanded random variables; For Gaussian process  $Y(t)$  here,  $\xi_i$  ( $i = 1, \dots, p$ ) are the standard normal variables;  $\lambda_i$  and  $\phi_i$  represent the dominated eigenvalues and eigenvectors, respectively.  $\boldsymbol{\rho}_Y(t) = [\sigma(t) \sigma(t_1) \rho(t, t_1), \dots, \sigma(t) \sigma(t_{n_t}) \rho(t, t_{n_t})]^\top$  denotes the vector of covariance function;  $\sigma(t)$  denotes the standard deviation function;  $\rho_Y(t_i, t_j)$  is the autocorrelation function.

## 2.3. TDFP estimation by MCS

After the stochastic processes  $\mathbf{Y}(t)$  are discretized, the LSF is expressed as  $g(\mathbf{x}, \mathbf{y}((\xi_1, \xi_2, \dots, \xi_m), t), t)$ , where  $\xi_i$  ( $i = 1, \dots, m$ ) denote the vectors of random variables. Based on MCS, the TDFP in Eq. (2) is estimated as:

$$\tilde{P}_f(0, t_e) = \frac{1}{N_{mcs}} \sum_{i=1}^{N_{mcs}} I_t(\mathbf{x}^{(i)}, (\xi_1^{(i)}, \xi_2^{(i)}, \dots, \xi_m^{(i)})) \quad (5)$$

where  $N_{mcs}$  denotes the number of samples; The indicator function  $I_t(\mathbf{x}^{(i)}, (\xi_1^{(i)}, \xi_2^{(i)}, \dots, \xi_m^{(i)}))$  is expressed as:

$$I_t(\mathbf{x}^{(i)}, (\xi_1^{(i)}, \xi_2^{(i)}, \dots, \xi_m^{(i)})) = \begin{cases} 1, & \text{if } g(\mathbf{x}^{(i)}, \mathbf{y}((\xi_1^{(i)}, \xi_2^{(i)}, \dots, \xi_m^{(i)}), t_j), t_j) < 0, \exists j = 1, \dots, n_t \\ 0, & \text{otherwise} \end{cases} \quad (6)$$

The coefficient of variation (COV) of  $\tilde{P}_f(0, t_e)$  is written as:

$$\text{COV}(\tilde{P}_f(0, t_e)) = \sqrt{\frac{1 - \tilde{P}_f(0, t_e)}{(N_{mcs} - 1) \times \tilde{P}_f(0, t_e)}} \quad (7)$$

It should be noted that the MCS involves a double loop computation procedure. That is, the realizations  $\{\mathbf{x}^{(i)}, (\xi_1^{(i)}, \xi_2^{(i)}, \dots, \xi_m^{(i)})\}_{i=1}^{N_{mcs}}$  are first generated in the outer loop. For any realization, the LSF is evaluated at  $n_t$  time instants in the inner loop, i.e.,  $\{g(\mathbf{x}^{(i)}, \mathbf{y}((\xi_1^{(i)}, \xi_2^{(i)}, \dots, \xi_m^{(i)}), t_j), t_j)\}_{j=1}^{n_t}$ . If the minimum response is less than zero (i.e.,  $\min\left(\{g(\mathbf{x}^{(i)}, \mathbf{y}((\xi_1^{(i)}, \xi_2^{(i)}, \dots, \xi_m^{(i)}), t_j), t_j)\}_{j=1}^{n_t}\right) < 0$ ), the realization is regarded to be failed; otherwise, it is considered safe. A schematic representation of the MCS is given in Fig. 1, where the failed time trajectories are denoted by the red lines. The TDFP is calculated by dividing the number of failed time trajectories by the total number of time trajectories.

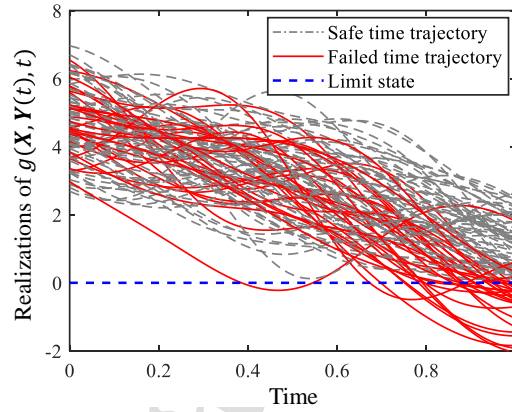


Figure 1: Illustrative diagram of MCS.

#### 2.4. Kriging-based global response surrogate method

The MCS-based TDFP estimation requires  $N_{mcs} \times n_t$  LSF evaluations, making it prohibitive in many practical engineering problems. To address this problem, the Kriging model is adopted to build a global response surrogate model for the LSF, enabling efficient estimation of the TDFP. The details of Kriging model is presented in Appendix A. The stochastic processes  $\mathbf{Y}(t)$  are expressed using  $\sum_{i=1}^m p^{(i)}$  random variables. Hence, the input dimension of LSF is equal to  $n + \sum_{i=1}^m p^{(i)} + 1$ . In order to avoid dealing with high dimensions, the stochastic processes are directly used as inputs of the Kriging model, instead of the



expanded random variables. The input dimension is thus reduced to  $n + m + 1$ . The transformation of input can be given as:

$$\begin{bmatrix} \mathbf{x}^{(1)} & (\boldsymbol{\xi}_1^{(1)}, \dots, \boldsymbol{\xi}_m^{(1)}) & t^{(1)} \\ \mathbf{x}^{(2)} & (\boldsymbol{\xi}_1^{(2)}, \dots, \boldsymbol{\xi}_m^{(2)}) & t^{(2)} \\ \vdots & \vdots & \vdots \\ \mathbf{x}^{(n_0)} & (\boldsymbol{\xi}_1^{(n_0)}, \dots, \boldsymbol{\xi}_m^{(n_0)}) & t^{(n_0)} \end{bmatrix} \rightarrow \text{Eq. (4)} \rightarrow \begin{bmatrix} \mathbf{x}^{(1)} & \mathbf{y}_t^{(1)} & t^{(1)} \\ \mathbf{x}^{(2)} & \mathbf{y}_t^{(2)} & t^{(2)} \\ \vdots & \vdots & \vdots \\ \mathbf{x}^{(n_0)} & \mathbf{y}_t^{(n_0)} & t^{(n_0)} \end{bmatrix} \quad (8)$$

where  $n_0$  is the number of training points.

The adaptive Kriging based TRA methods starts with constructing a rough Kriging surrogate model with a small number of initial training points. Then, new informative training points are sequentially selected through a learning function and the Kriging model is updated. The procedure is terminated when a predefined stopping criterion is fulfilled. Finally, the TDFP is estimated as:

$$\hat{P}_f(0, t_e) = \frac{1}{N_{mcs}} \sum_{i=1}^{N_{mcs}} \hat{I}_t(\mathbf{x}^{(i)}, \mathbf{y}_t^{(i)}) \quad (9)$$

where  $\hat{I}_t(\mathbf{x}^{(i)}, \mathbf{y}_t^{(i)})$  is denoted as:

$$\hat{I}_t(\mathbf{x}^{(i)}, \mathbf{y}_t^{(i)}) = \begin{cases} 1, & \text{if } \mu_{\hat{g}}(\mathbf{x}^{(i)}, \mathbf{y}_{t_j}^{(i)}, t_j) < 0, \exists j = 1, \dots, n_t \\ 0, & \text{otherwise} \end{cases} \quad (10)$$

where  $\mu_{\hat{g}}(\mathbf{x}^{(i)}, \mathbf{y}_{t_j}^{(i)}, t_j)$  is the mean prediction of the Kriging model.

### 3. Error-informed Parallel Adaptive Kriging

This section proposes a new method called EPAK, which can estimate small TDFPs and enable parallel computing. First, the VAIS is adapted in a sequential way to reduce the sample size and computational cost. Later, the maximum relative error of TDFP is derived under the combination of Kriging model and

VAIS. Finally, a stopping criterion and a parallel sampling strategy are developed to adaptively enrich the training point set.

### 3.1. Sequential variance-amplified importance sampling

As mentioned in the last section, MCS involves a double loop computation procedure and requires  $N_{mcs} \times n_t$  Kriging model predictions. For problems with low TDFPs, a large  $N_{mcs}$  should be specified to ensure the estimation accuracy, rendering the computation cumbersome. To address this problem, the VAIS developed in [48] is introduced and adapted in a sequential way to replace the MCS in this study, so as to reduce the sample size and total computation time.

The TDFP  $P_f(0, t_e)$  in Eq. (2) is rewritten as:

$$P_f(0, t_e) = \int_{\mathbb{R}^n} \int_{\mathbb{R}^\infty} I(\mathbf{x}, \mathbf{y}(\boldsymbol{\xi}, t), t) \frac{f_{\mathbf{X}}(\mathbf{x})}{h_{\mathbf{X}}(\mathbf{x})} h_{\mathbf{X}}(\mathbf{x}) f_{\Xi}(\boldsymbol{\xi}) d\mathbf{x} d\boldsymbol{\xi} \quad (11)$$

where  $h_{\mathbf{X}}(\mathbf{x}) = f_{\mathbf{X}}(\mathbf{x}; \mathbf{m}_{\mathbf{X}}, \gamma \cdot \boldsymbol{\sigma}_{\mathbf{X}})$  denotes the importance sampling density (ISD), which is established by enlarging the vector of standard deviations  $\boldsymbol{\sigma}_{\mathbf{X}}$  (or enlarging the vector of variances  $\boldsymbol{\sigma}_{\mathbf{X}}^2$ ) of the PDF  $f_{\mathbf{X}}(\mathbf{x})$  (maintain the means  $\mathbf{m}_{\mathbf{X}}$  unchanged), where  $\gamma$  is the amplification factor. Note that the stochastic processes are typically represented by many random variables, and amplifying the standard deviations of these random variables greatly increases the computational complexity. For simplicity, only the standard deviations of input random variables in LSF are amplified.

Then,  $\Delta N$  samples are generated from  $h_{\mathbf{X}}(\mathbf{x})$  and  $f_{\Xi}(\boldsymbol{\xi})$ .  $P_f(0, t_e)$  in Eq. (11) can be estimated as:

$$\hat{P}_f(0, t_e) = \frac{1}{\Delta N} \sum_{i=1}^{\Delta N} \hat{I}_t(\mathbf{x}^{(i)}, \mathbf{y}_t^{(i)}) \frac{f_{\mathbf{X}}(\mathbf{x}^{(i)})}{h_{\mathbf{X}}(\mathbf{x}^{(i)})} \quad (12)$$

The variance and COV of  $\hat{P}_f(0, t_e)$  are given as:

$$\mathbb{V}[\hat{P}_f(0, t_e)] = \frac{1}{\Delta N - 1} \left( \frac{1}{\Delta N} \sum_{i=1}^{\Delta N} \hat{I}_t(\mathbf{x}^{(i)}, \mathbf{y}_t^{(i)}) \left( \frac{f_{\mathbf{X}}(\mathbf{x}^{(i)})}{h_{\mathbf{X}}(\mathbf{x}^{(i)})} \right)^2 - \left( \hat{P}_f(0, t_e) \right)^2 \right) \quad (13)$$

$$\mathbb{COV} [\hat{P}_f(0, t_e)] = \frac{\sqrt{\mathbb{V} [\hat{P}_f(0, t_e)]}}{\hat{P}_f(0, t_e)} \quad (14)$$

The samples are generated sequentially from the ISD and  $f_{\Xi}(\xi)$ , and then predicted on the Kriging model, which can greatly save the computation time. First,  $\Delta N$  samples are generated. Let the number of iteration  $s = 1$  and the total number of samples  $N_0 = s \times \Delta N$ . The TDFP is estimated by Eq. (12) and expressed as  $\hat{P}_f^{(s)}$ . A quantity  $\varpi^{(s)}$  is introduced to efficiently store the Kriging prediction information for  $\Delta N$  samples, minimizing memory usage while enabling the calculation of the variance estimator.  $\varpi^{(s)}$  is written as:

$$\varpi^{(s)} = \frac{1}{\Delta N} \sum_{i=1}^{\Delta N} \hat{I}_t(\mathbf{x}^{(i)}, \mathbf{y}_t^{(i)}) \left( \frac{f_{\mathbf{X}}(\mathbf{x}^{(i)})}{h_{\mathbf{X}}(\mathbf{x}^{(i)})} \right)^2 \quad (15)$$

Additional  $\Delta N$  samples are generated and let  $s = s + 1$ .  $\hat{P}_f^{(s)}$  and  $\varpi^{(s)}$  are estimated by Eq. (12) and Eq. (15), respectively. The TDFP and its variance can be re-estimated as:

$$\hat{P}_f(0, t_e) = \frac{1}{s} \sum_{i=1}^s \hat{P}_f^{(s)} \quad (16)$$

$$\mathbb{V} [\hat{P}_f(0, t_e)] = \frac{1}{N_0 - 1} \left( \frac{1}{s} \sum_{i=1}^s \varpi^{(s)} - \left( \hat{P}_f(0, t_e) \right)^2 \right) \quad (17)$$

The sampling process is executed until the COV of the TDFP is lower than the target threshold, i.e.,  $\mathbb{COV} [\hat{P}_f(0, t_e)] < \epsilon_p$ .

### 3.2. Relative error of TDFP

According to Eq. (10),  $\hat{I}_t(\mathbf{x}^{(i)}, \mathbf{y}_t^{(i)})$  is estimated based on judging the sign of  $\mu_{\hat{g}}(\mathbf{x}^{(i)}, \mathbf{y}_t^{(i)}, t)$ , which is predicted by Kriging and may be wrongly estimated. The relative error of the predicted TDFP  $\hat{P}_f(0, t_e)$  with respect to the true result  $P_f(0, t_e)$  can be defined as:

$$\delta = \left| \frac{P_f(0, t_e) - \hat{P}_f(0, t_e)}{P_f(0, t_e)} \right| \quad (18)$$

The true result  $P_f(0, t_e)$  is expressed as:

$$P_f(0, t_e) = \frac{1}{N_0} \left[ \sum_{i=1}^{N_0} \hat{I}_t(\mathbf{x}^{(i)}, \mathbf{y}_t^{(i)}) \frac{f_{\mathbf{X}}(\mathbf{x}^{(i)})}{h_{\mathbf{X}}(\mathbf{x}^{(i)})} + \sum_{h=1}^{\hat{N}_s^w} \frac{f_{\mathbf{X}}(\mathbf{x}^{(h)})}{h_{\mathbf{X}}(\mathbf{x}^{(h)})} - \sum_{k=1}^{\hat{N}_f^w} \frac{f_{\mathbf{X}}(\mathbf{x}^{(k)})}{h_{\mathbf{X}}(\mathbf{x}^{(k)})} \right] \quad (19)$$

where  $\hat{N}_s^w$  denotes the total number of time trajectories predicted to be safe by Kriging model but misclassified;  $\hat{N}_f^w$  denotes the total number of time trajectories predicted to be failed but misclassified. Due to the fact that the true number of misclassified time trajectories is unknown, the last two terms in Eq. (19) are uncertain. Let  $\sum_{h=1}^{\hat{N}_s^w} \frac{f_{\mathbf{X}}(\mathbf{x}^{(h)})}{h_{\mathbf{X}}(\mathbf{x}^{(h)})} = \mathcal{N}_s$  and  $\sum_{k=1}^{\hat{N}_f^w} \frac{f_{\mathbf{X}}(\mathbf{x}^{(k)})}{h_{\mathbf{X}}(\mathbf{x}^{(k)})} = \mathcal{N}_f$ , the relative error  $\delta$  can thus be written as:

$$\delta = \left| 1 - \frac{\sum_{i=1}^{N_0} \hat{I}_t(\mathbf{x}^{(i)}, \mathbf{y}_t^{(i)}) \frac{f_{\mathbf{X}}(\mathbf{x}^{(i)})}{h_{\mathbf{X}}(\mathbf{x}^{(i)})}}{\sum_{i=1}^{N_0} \hat{I}_t(\mathbf{x}^{(i)}, \mathbf{y}_t^{(i)}) \frac{f_{\mathbf{X}}(\mathbf{x}^{(i)})}{h_{\mathbf{X}}(\mathbf{x}^{(i)})} + \mathcal{N}_s - \mathcal{N}_f} \right| \quad (20)$$

Although the exact values of  $\mathcal{N}_s$  and  $\mathcal{N}_f$  are unknown, it is possible to obtain the expectation and variance of the two quantities. To achieve this goal,  $\hat{I}_t^s(\mathbf{x}^{(h)}, \mathbf{y}_t^{(h)}) = 1$  is first introduced to denote that the time trajectory predicted to be safe by Kriging is actually in a failed status. Correspondingly,  $\hat{I}_t^s(\mathbf{x}^{(h)}, \mathbf{y}_t^{(h)}) = 0$  denotes that the time trajectory predicted to be safe is correctly classified.  $\mathcal{N}_s$  can thus be written as:

$$\mathcal{N}_s = \sum_{h=1}^{\hat{N}_s^w} \frac{f_{\mathbf{X}}(\mathbf{x}^{(h)})}{h_{\mathbf{X}}(\mathbf{x}^{(h)})} = \sum_{h=1}^{N_s} \hat{I}_t^s(\mathbf{x}^{(h)}, \mathbf{y}_t^{(h)}) \frac{f_{\mathbf{X}}(\mathbf{x}^{(h)})}{h_{\mathbf{X}}(\mathbf{x}^{(h)})} \quad (21)$$

where  $N_s$  is the total number of safe time trajectory predicted by Kriging.

The expectation and variance of  $\mathcal{N}_s$  can be expressed as:

$$\mathbb{E}[\mathcal{N}_s] = \mathbb{E} \left[ \sum_{h=1}^{N_s} \hat{I}_t^s(\mathbf{x}^{(h)}, \mathbf{y}_t^{(h)}) \frac{f_{\mathbf{X}}(\mathbf{x}^{(h)})}{h_{\mathbf{X}}(\mathbf{x}^{(h)})} \right] = \sum_{h=1}^{N_s} \mathbb{E} \left[ \hat{I}_t^s(\mathbf{x}^{(h)}, \mathbf{y}_t^{(h)}) \right] \frac{f_{\mathbf{X}}(\mathbf{x}^{(h)})}{h_{\mathbf{X}}(\mathbf{x}^{(h)})} \quad (22)$$

$$\mathbb{V}[\mathcal{N}_s] = \mathbb{V} \left[ \sum_{h=1}^{N_s} \hat{I}_t^s(\mathbf{x}^{(h)}, \mathbf{y}_t^{(h)}) \frac{f_{\mathbf{X}}(\mathbf{x}^{(h)})}{h_{\mathbf{X}}(\mathbf{x}^{(h)})} \right] = \sum_{h=1}^{N_s} \mathbb{V} \left[ \hat{I}_t^s(\mathbf{x}^{(h)}, \mathbf{y}_t^{(h)}) \right] \left( \frac{f_{\mathbf{X}}(\mathbf{x}^{(h)})}{h_{\mathbf{X}}(\mathbf{x}^{(h)})} \right)^2 \quad (23)$$

where the probability of  $\hat{I}_t^s(\mathbf{x}^{(h)}, \mathbf{y}_t^{(h)}) = 0$ , i.e., the probability of correct sign estimate of  $(\mathbf{x}^{(h)}, \mathbf{y}_t^{(h)})$ , can

213 be expressed as:

$$p_{s,c}(\mathbf{x}^{(h)}, \mathbf{y}_t^{(h)}) = \mathbb{P}\left\{\hat{I}_t^s(\mathbf{x}^{(h)}, \mathbf{y}_t^{(h)}) = 0\right\} = \mathbb{P}\left\{\bigcap_{h=1}^{n_t} \hat{g}(\mathbf{x}^{(h)}, \mathbf{y}_{t_j}^{(h)}, t_j) > 0\right\} \quad (24)$$

214 where the computation of  $p_{s,c}(\mathbf{x}^{(h)}, \mathbf{y}_t^{(h)})$  is quite cumbersome in practice. Instead of calculating the  
 215 exact value of the  $p_{s,c}(\mathbf{x}^{(h)}, \mathbf{y}_t^{(h)})$ , it is possible to obtain its sub-optimal estimate without sacrificing the  
 216 estimation accuracy according to our recent study [46]. The sub-optimal estimate  $\bar{p}_{s,c}(\mathbf{x}^{(h)}, \mathbf{y}_t^{(h)})$  can be  
 217 expressed as [46]:

$$\bar{p}_{s,c}(\mathbf{x}^{(h)}, \mathbf{y}_t^{(h)}) = \min_{j=1, \dots, n_t} \Phi\left(\frac{\mu_{\hat{g}}(\mathbf{x}^{(h)}, \mathbf{y}_{t_j}^{(h)}, t_j)}{\sigma_{\hat{g}}(\mathbf{x}^{(h)}, \mathbf{y}_{t_j}^{(h)}, t_j)}\right) \quad (25)$$

218 The sub-optimal estimate of misclassification probability is written as:

$$\bar{p}_{s,w}(\mathbf{x}^{(h)}, \mathbf{y}_t^{(h)}) = \mathbb{P}\left\{\hat{I}_t^s(\mathbf{x}^{(h)}, \mathbf{y}_t^{(h)}) = 1\right\} = 1 - \min_{j=1, \dots, n_t} \Phi\left(\frac{\mu_{\hat{g}}(\mathbf{x}^{(h)}, \mathbf{y}_{t_j}^{(h)}, t_j)}{\sigma_{\hat{g}}(\mathbf{x}^{(h)}, \mathbf{y}_{t_j}^{(h)}, t_j)}\right) \quad (26)$$

219 It is easy to find that  $\hat{I}_t^s(\mathbf{x}^{(h)}, \mathbf{y}_t^{(h)})$  follows the Bernoulli distribution. The expectation and variance of  
 220  $\mathcal{N}_s$  are rewritten as:

$$\mathbb{E}[\mathcal{N}_s] = \sum_{h=1}^{N_s} \bar{p}_{s,w}(\mathbf{x}^{(h)}, \mathbf{y}_t^{(h)}) \frac{f_{\mathbf{X}}(\mathbf{x}^{(h)})}{h_{\mathbf{X}}(\mathbf{x}^{(h)})} \quad (27)$$

$$\mathbb{V}[\mathcal{N}_s] = \sum_{h=1}^{N_s} \bar{p}_{s,w}(\mathbf{x}^{(h)}, \mathbf{y}_t^{(h)}) \left(1 - \bar{p}_{s,w}(\mathbf{x}^{(h)}, \mathbf{y}_t^{(h)})\right) \left(\frac{f_{\mathbf{X}}(\mathbf{x}^{(h)})}{h_{\mathbf{X}}(\mathbf{x}^{(h)})}\right)^2 \quad (28)$$

222 Similarly, let  $\hat{I}_t^f(\mathbf{x}^{(k)}, \mathbf{y}_t^{(k)}) = 1$  denote that the time trajectory predicted to be failed by Kriging is  
 223 actually in a safe status. Correspondingly,  $\hat{I}_t^s(\mathbf{x}^{(k)}, \mathbf{y}_t^{(k)}) = 0$  denotes the time trajectory predicted to be  
 224 failed is correctly classified.

225 The misclassification probability can be written as:

$$p_{f,w}(\mathbf{x}^{(k)}, \mathbf{y}_t^{(k)}) = \mathbb{P}\left\{\hat{I}_t^f(\mathbf{x}^{(k)}, \mathbf{y}_t^{(k)}) = 1\right\} = \mathbb{P}\left\{\bigcap_{j=1}^{n_t} \hat{g}(\mathbf{x}^{(k)}, \mathbf{y}_{t_j}^{(k)}, t_j) > 0\right\} \quad (29)$$

226 According to the aforementioned discussion, the corresponding sub-optimal estimate of  $p_{f,w}(\mathbf{x}^{(k)}, \mathbf{y}_t^{(k)})$   
 227 can be defined as:

$$\bar{p}_{f,w}(\mathbf{x}^{(k)}, \mathbf{y}_t^{(k)}) = \min_{j=1, \dots, n_t} \Phi \left( \frac{\mu_{\hat{g}}(\mathbf{x}^{(k)}, \mathbf{y}_{t_j}^{(k)}, t_j)}{\sigma_{\hat{g}}(\mathbf{x}^{(k)}, \mathbf{y}_{t_j}^{(k)}, t_j)} \right) \quad (30)$$

228 The expectation and variance of  $\mathcal{N}_f$  can be written as:

$$\mathbb{E}[\mathcal{N}_f] = \sum_{k=1}^{N_f} \bar{p}_{f,w}(\mathbf{x}^{(k)}, \mathbf{y}_t^{(k)}) \frac{f_{\mathbf{X}}(\mathbf{x}^{(k)})}{h_{\mathbf{X}}(\mathbf{x}^{(k)})} \quad (31)$$

$$\mathbb{V}[\mathcal{N}_f] = \sum_{k=1}^{N_f} \bar{p}_{f,w}(\mathbf{x}^{(k)}, \mathbf{y}_t^{(k)}) \left(1 - \bar{p}_{f,w}(\mathbf{x}^{(k)}, \mathbf{y}_t^{(k)})\right) \left(\frac{f_{\mathbf{X}}(\mathbf{x}^{(k)})}{h_{\mathbf{X}}(\mathbf{x}^{(k)})}\right)^2 \quad (32)$$

230 where  $N_f$  is the total number of failed points predicted by Kriging model.

231 For any time trajectory predicted to be either safe or failed, the sub-optimal estimate of the misclassifi-  
 232 cation probability is expressed as:

$$\bar{p}_w(\mathbf{x}^{(i)}, \mathbf{y}_t^{(i)}) = \Phi \left( - \left| \min_{j=1, \dots, n_t} \frac{\mu_{\hat{g}}(\mathbf{x}^{(i)}, \mathbf{y}_{t_j}^{(i)}, t_j)}{\sigma_{\hat{g}}(\mathbf{x}^{(i)}, \mathbf{y}_{t_j}^{(i)}, t_j)} \right| \right) \quad (33)$$

233 With the VAIS technique presented in Section 3.1, the dispersedly distributed samples are generated as  
 234 the candidate samples. It is reasonable to consider that the number of safe time trajectories  $N_s$  and the  
 235 number of failed time trajectories  $N_f$  are both large enough. In this case, the confidence intervals of  $\mathcal{N}_s$   
 236 and  $\mathcal{N}_f$  can be approximately obtained using the central limit theorem. Besides,  $\mathcal{N}_s$  and  $\mathcal{N}_f$  approximately  
 237 follow normal distributions, which are expressed as:

$$\mathcal{N}_s \sim N(\mathbb{E}[\mathcal{N}_s], \mathbb{V}[\mathcal{N}_s]) \quad (34)$$

$$\mathcal{N}_f \sim N(\mathbb{E}[\mathcal{N}_f], \mathbb{V}[\mathcal{N}_f]) \quad (35)$$

The confidence intervals of  $\mathcal{N}_s$  and  $\mathcal{N}_f$  can be obtained as:

$$\mathcal{N}_s \in [\mathcal{N}_s^l, \mathcal{N}_s^u] = [\Phi_{\mathcal{N}_s}^{-1}(\alpha/2), \Phi_{\mathcal{N}_s}^{-1}(1 - \alpha/2)] \quad (36)$$

$$\mathcal{N}_f \in [\mathcal{N}_f^l, \mathcal{N}_f^u] = [\Phi_{\mathcal{N}_f}^{-1}(\alpha/2), \Phi_{\mathcal{N}_f}^{-1}(1 - \alpha/2)] \quad (37)$$

where  $\Phi_{\mathcal{N}_s}^{-1}(\cdot)$  and  $\Phi_{\mathcal{N}_f}^{-1}(\cdot)$  denote inverse cumulative distribution functions (CDFs);  $\alpha$  is the confidence level ( $\alpha = 0.05$  is used in this study).

The maximum relative error of TDFP can thus be obtained by:

$$\delta_{\max} = \max \left( \left| \frac{\mathcal{N}_s^l - \mathcal{N}_f^u}{\sum_{i=1}^{N_0} \hat{I}_t(\mathbf{x}^{(i)}, \mathbf{y}_t^{(i)}) \frac{f_{\mathbf{x}}(\mathbf{x}^{(i)})}{h_{\mathbf{x}}(\mathbf{x}^{(i)})} + \mathcal{N}_s^l - \mathcal{N}_f^u} \right|, \left| \frac{\mathcal{N}_s^u - \mathcal{N}_f^l}{\sum_{i=1}^{N_0} \hat{I}_t(\mathbf{x}^{(i)}, \mathbf{y}_t^{(i)}) \frac{f_{\mathbf{x}}(\mathbf{x}^{(i)})}{h_{\mathbf{x}}(\mathbf{x}^{(i)})} + \mathcal{N}_s^u - \mathcal{N}_f^l} \right| \right) \quad (38)$$

It should be noted that the quantification of the relative error of TDFP can be regarded as an extension of the study in static reliability analysis [53] and the one in time-dependent reliability analysis [36]. The significant difference is that the estimation of relative error is based on the VAIS in this study, whereas it is based on MCS in the two existing studies.

### 3.3. Stopping criterion and parallel sampling strategy

In adaptive Kriging based TRA method, a suitable stopping criterion is required to determine whether the obtained estimate of TDFP is accurate enough as the final result. Based on the Eq. (38), the stopping criterion can be defined by judging whether the maximum relative error of TDFP is below a prescribed threshold:

$$\delta_{\max} \leq \epsilon_r \quad (39)$$

where  $\epsilon_r$  is the specified threshold. Note that the adaptive updating of Kriging model is terminated only when Eq. (39) is satisfied twice consecutively to prevent the potential fake convergence.

If the stopping criterion is not met, new training points need to be identified and evaluated on the true LSF to update the Kriging model. In order to efficiently decrease the maximum relative error of TDFP,

the number of misclassified time trajectories should be as small as possible. In other words, the greater the misclassification of a time trajectory, the greater the contribution to reducing the relative error of TDFP. That is, the  $\bar{p}_w(\mathbf{x}, \mathbf{y}_t)$  in Eq. (33) measures the contribution of the time trajectory to the relative error of TDFP. Therefore, the relative error can be minimized as much as possible through evaluating the point that maximizes the misclassification probability in Eq. (33). However, directly selecting the point with the highest misclassification probability overlooks the distance between the newly added training point and the existing ones, which may cause excessive clustering and lead to unnecessary LSF evaluations. To address this problem, this paper introduces a influence function by considering the correlation between the existing training points and all candidate points as the distance measure, and then proposes a new learning function called improved relative error contribution (IREC):

$$\text{IREC}(\mathbf{x}, \mathbf{y}_t) = IF(\mathbf{x}; \mathbf{x}^{(1)}, \mathbf{x}^{(2)}, \dots, \mathbf{x}^{(n_0)}) \times \bar{p}_w(\mathbf{x}, \mathbf{y}_t) \quad (40)$$

where  $IF(\mathbf{x}; \mathbf{x}^{(1)}, \mathbf{x}^{(2)}, \dots, \mathbf{x}^{(n_0)})$  is the introduced influence function and denoted as [54]:

$$IF(\mathbf{x}; \mathbf{x}^{(1)}, \mathbf{x}^{(2)}, \dots, \mathbf{x}^{(n_0)}) = \prod_{i=1}^{n_0} [1 - R(\mathbf{x}, \mathbf{x}^{(i)})] \quad (41)$$

where  $\mathbf{x}^{(1)}, \mathbf{x}^{(2)}, \dots, \mathbf{x}^{(n_0)}$  are the  $n_0$  existing training points;  $R(\cdot)$  is the Gaussian correlation function of the Kriging model in this study.

The IREC function can be further extended to parallel sampling case by exploiting the advantages of the introduced influence function. In an active learning iteration,  $q$  training points are sequentially selected and simultaneously enriched to the dataset  $\mathcal{D}$ , which is elaborated as follows. First, the time trajectory maximizing the IREC function is selected and then the time instant with the largest prediction uncertainty is chosen. Herein, the commonly used U function is used to determine the optimal time instant [55]. Therefore,



the selection strategy of the first added training point  $\mathbf{v}_{new}^{(n_0+1)}$  is expressed as follows:

$$\mathbf{v}_{new}^{(n_0+1)} = [\mathbf{x}^{(i^*)}, \mathbf{y}_{t_{j^*}}^{(i^*)}, t_{j^*}]$$

$$i^* = \arg \max_{i=1, \dots, N_0} IF(\mathbf{x}; \mathbf{x}^{(1)}, \mathbf{x}^{(2)}, \dots, \mathbf{x}^{(n_0)}) \bar{p}_w(\mathbf{x}^{(i)}, \mathbf{y}_t^{(i)}), \quad j^* = \arg \min_{j=1, \dots, n_t} \frac{|\mu_{\hat{g}}(\mathbf{x}^{(i^*)}, \mathbf{y}_{t_{j^*}}^{(i^*)}, t_j)|}{\sigma_{\hat{g}}(\mathbf{x}^{(i^*)}, \mathbf{y}_{t_{j^*}}^{(i^*)}, t_j)} \quad (42)$$

Sequentially, after  $q - 1$  updated training points have been identified, the  $q$ -th training point can be obtained as:

$$\mathbf{v}_{new}^{(n_0+q)} = [\mathbf{x}^{(i^*)}, \mathbf{y}_{t_{j^*}}^{(i^*)}, t_{j^*}]$$

$$i^* = \arg \max_{i=1, \dots, N_0} IF(\mathbf{x}; \mathbf{x}^{(1)}, \mathbf{x}^{(2)}, \dots, \mathbf{x}^{(n_0+q-1)}) \bar{p}_w(\mathbf{x}^{(i)}, \mathbf{y}_t^{(i)}), \quad j^* = \arg \min_{j=1, \dots, n_t} \frac{|\mu_{\hat{g}}(\mathbf{x}^{(i^*)}, \mathbf{y}_{t_{j^*}}^{(i^*)}, t_j)|}{\sigma_{\hat{g}}(\mathbf{x}^{(i^*)}, \mathbf{y}_{t_{j^*}}^{(i^*)}, t_j)} \quad (43)$$

It is evident from Eqs. (42)-(43) that  $q$  training points are sequentially identified through considering the relative error contribution and the correlation between all training points and candidate points. After  $q$  training points are selected within an iteration, the Kriging model is updated. Note that the developed parallel sampling strategy may be similar to the idea that multiple informative points are sequentially generated by maximizing the product of the learning function and influence function, which is recently introduced in the field of time-invariant reliability analysis [56, 57] and time-dependent system reliability analysis [58]. The difference lies mainly in two aspects. First, this study develops a new IREC learning function based on the concept of minimizing the relative error of TDFP. Second, the several existing researches have only considered the correlation between the current and previously selected points within an iteration, ignoring the correlation of the training points prior to the current iteration, whereas this study addresses this problem.

### 3.4. Implementation of the proposed method

The flowchart of the proposed method is shown in Fig. 2. The implementation procedures are summarized as follows:

**Step 1:** Discretize the time interval  $[0, t_e]$  and the stochastic processes  $\mathbf{Y}(t)$  (if involved).

**Step 2:** Generate  $n_0$  initial training points by Sobol sequence. The sampling domain of these initial points is set to  $[\boldsymbol{\mu} - 3\boldsymbol{\sigma}, \boldsymbol{\mu} + 3\boldsymbol{\sigma}]$ , where  $\boldsymbol{\mu}$  and  $\boldsymbol{\sigma}$  are the mean and standard deviation of the input random

variables, respectively. The corresponding responses are calculated by evaluating the LSF  $g(\cdot)$ . Establish the initial dataset  $\mathcal{D} = \{[\mathbf{x}^{(i)}, \mathbf{y}_{t_i}^{(i)}, t_i], g^{(i)}\}_{i=1}^{n_0}$  with the EOLE method. Let the number of LSF evaluations  $N_{eva} = n_0$  and the number of iterations  $N_{ite} = 1$ .

**Step 3:** Construct the candidate sample pool  $\mathcal{S} = [\mathbf{x}^{(i)}, (\boldsymbol{\xi}_1^{(i)}, \dots, \boldsymbol{\xi}_m^{(i)})]_{i=1}^{\Delta N}$ , where  $\Delta N$  is the number of initial candidate samples. Let  $s = 1$  and the the number of total candidate samples  $N_0 = s \times \Delta N$ .

**Step 4:** Build the Kriging model based on the dataset  $\mathcal{D}$ .

**Step 5:** Estimate the TDFP  $\hat{P}_f(0, t_e)$  and its variance  $\mathbb{V}[\hat{P}_f(0, t_e)]$  based on Eqs. (16)-(17). Calculate the maximum relative error  $\delta_{\max}$  in Eq. (38).

**Step 6:** If the stopping criterion in Eq. (39) is fulfilled twice consecutively, turn to Step 8; else, turn to Step 7.

**Step 7:** Identify  $q$  points  $\mathcal{D}_+ = [\mathbf{x}^{(i)}, \mathbf{y}_{t_i}^{(i)}, t_i]_{i=1}^q$  using the developed parallel sampling strategy. Evaluate the LSF on the  $q$  selected points to obtain the responses  $\{g^{(i)}\}_{i=1}^q$ . Enrich the points and responses into the dataset  $\mathcal{D}$ . Let  $N_{eva} = N_{eva} + q$  and  $N_{ite} = N_{ite} + 1$ , and return to Step 4.

**Step 8:** Check if the COV of the TDFP is below the target threshold, i.e,  $\mathbb{COV}[\hat{P}_f(0, t_e)] < \epsilon_p$ . If satisfied, go to Step 9; else, generate additional  $\Delta N$  candidate samples and enrich the candidate sample pool  $\mathcal{S}$ , let  $s = s + 1$  and return to Step 5.

**Step 9:** Return the estimated TDFP  $\hat{P}_f(0, t_e)$  and end the proposed method.

#### 4. Examples and results

The effectiveness of the proposed EPAK method is validated by comparing it with several existing non-parallel TRA methods. The two compared methods, SILK [33] and REAL [36], are implemented in all examples and the number of initial training points is set to be 12. Other implementation details follow the default settings in the original studies. The results for the remaining compared methods, including eSPT [59], STRA [60], SLK-co-SS [45], etc., are taken from the respective publications unless otherwise stated. The parameter settings for the proposed method are as follows:  $n_0 = 12$ ,  $\gamma = 1.5$ ,  $\Delta N = 10^4$ ,  $\epsilon_p = 5\%$ ,  $\epsilon_r = 5\%$ . Different values are specified for  $q$  to investigate the impact on the results. The reported results are

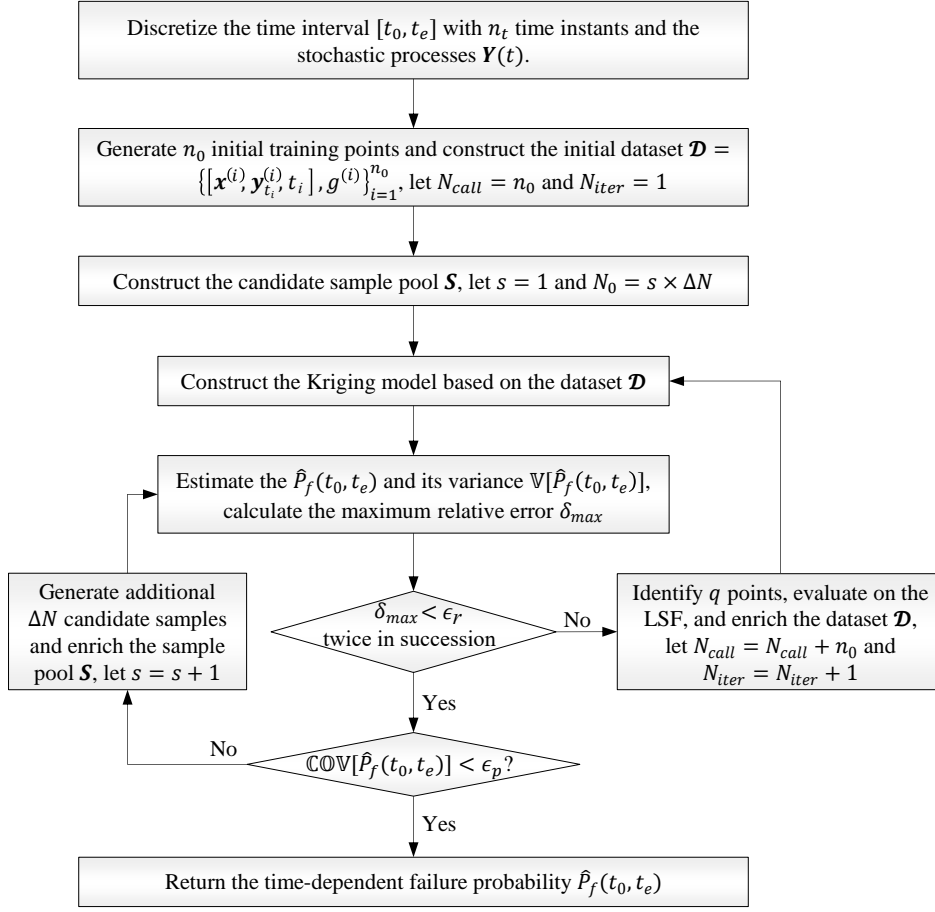


Figure 2: Flowchart of the proposed method.

319 averaged over 10 independent runs in MATLAB R2019(b) under the environment (CPU of Intel i5-13400F,  
 320 RAM of 16 GB) unless otherwise stated.

#### 321 4.1. Mathematical example

322 A mathematical model is investigated in this section [45, 59, 60]. The LSF is expressed as:

$$g(\mathbf{X}, Y(t), t) = X_1^2 X_2 + (X_2 + 1)t^2 - 5X_1(1 + Y(t))t - 20 \quad (44)$$

323 where the input variables  $X_1$  and  $X_2$  both follow a normal distribution with the mean of 3.5 and the standard  
 324 deviation of 0.25;  $Y(t)$  denotes a Gaussian process, where the mean and standard deviation are 0 and 1,

respectively. The autocorrelation function of the Gaussian process is defined as  $\kappa(t_1, t_2) = \exp[-(t_1 - t_2)^2]$ ;  $t \in [0, 1]$  represents the time parameter.

The time interval and Gaussian process  $Y(t)$  are discretized with 101 time instants and three independent standard normal variables, respectively. Fig. 3 depicts one hundred realizations of  $Y(t)$ . The TDFP results provided by different methods are listed in Table 1. The TDFP  $\hat{P}_f = 0.3079$  by MCS is considered as the reference result. It is observed that all methods can produce results close to the reference result. In terms of efficiency, the proposed method requires fewer iterations with the help of the developed parallel sampling strategy. When  $q = 1$  (indicating that the parallel computing is unavailable), the proposed method costs less LSF evaluations than other compared methods though it produces slightly larger COVs. Through comparing the computation time between different methods, it can be found that the proposed method typically requires less CPU time than other active learning TRA methods.

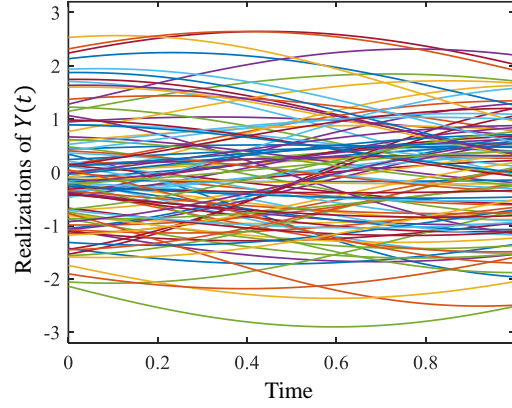
Table 1: TRA results of example 4.1.

Methods		$N_{ite}$	$N_{eva}$	$\hat{P}_f$	$\epsilon_{\hat{P}_f}$	$\text{COV}[\hat{P}_f]$	CPU Time (s)
MCS		-	$101 \times 10^6$	0.3079	-	0.15%	1.9
eSPT <sup>1</sup>		-	139	0.2986	3.02%	-	-
STRA <sup>2</sup>		16.4	27.4	0.3041	1.23%	-	-
SLK-co-SS <sup>3</sup>		35.8	46.8	0.3072	0.23%	-	-
SILK		12.5	23.5	0.3075	0.13%	2.95%	31.1
REAL		10.8	21.8	0.3070	0.29%	3.56%	29.5
Proposed method	$q = 1$	6.6	17.6	0.3059	0.65%	6.58%	2.5
	$q = 2$	4.3	18.6	0.2995	2.73%	7.02%	2.0
	$q = 3$	4.1	21.3	0.3014	2.11%	5.16%	2.2
	$q = 4$	3.7	22.8	0.3062	0.55%	4.16%	2.2
	$q = 5$	3.8	23.2	0.3031	1.56%	4.95%	2.3
	$q = 6$	3.5	27.0	0.3093	0.45%	3.14%	2.6
	$q = 7$	2.8	24.6	0.3086	0.23%	2.57%	2.2
	$q = 8$	2.8	26.4	0.3081	0.07%	3.51%	2.4

<sup>1</sup> The results are taken from research [59];<sup>2</sup> The results are taken from research [60];<sup>3</sup> The results are taken from research [45].

#### 4.2. Corroded simply supported beam

In this section, we consider the TRA of a corroded beam [60] shown in Fig 4. The span of the beam is 5m. The bending loads include the concentrated load  $F(t)$  and the uniformly distributed load  $p =$

Figure 3: Realizations of  $Y(t)$  of example 4.1.

339  $7.85 \times 10^4 b_0 h_0 (N/m)$ . The LSF is defined as follows:

$$g(\mathbf{x}, F(t), t) = \frac{(b_0 - 2\kappa t)[h_0 - 2\kappa t]^2 f_y}{4} - \left( \frac{F(t)L}{4} + \frac{7.85 \times 10^4 b_0 h_0 L^2}{8} \right) \quad (45)$$

340 where  $\kappa = 3 \times 10^{-5} \text{m/year}$  control the corrosion rate and  $t \in [0, 20]$  years represents time parameter;  $b_0$ ,  $h_0$   
 341 and  $f_y$  are the initial width and height of the cross section, and the yield strength, respectively. Table 2  
 342 lists the details of the random parameters.

343 The time interval  $[0, 12]$  and Gaussian process  $F(t)$  are discretized with 241 time instants and six inde-  
 344 pendent standard normal variables, respectively. The TRA results provided by different methods are listed  
 345 in Table 3. One can observe that all investigated methods can yield the results close to the reference value  
 346 provided by MCS. In terms of the efficiency, however, the proposed method requires much less iterations and  
 347 LSF evaluations than other methods. The comparison of computation time shows that the proposed method  
 348 requires less CPU time than both REAL and SILK methods. When  $q$  varies from 1 to 8 in the proposed  
 349 method, the number of LSF evaluations gradually increases. Besides, the proposed method requires the  
 350 least number of iterations and computation time for the setting of  $q = 5$ . This observation indicates that  
 351 selecting too many training points per iteration does not necessarily result in a reduction in the the number  
 352 of iterations and the total computation time.

353 Fig. 5 schematically presents the TDFP within the time interval  $[0, 20]$  years, where the error bar indicate

the range of the mean  $\pm 2$  standard deviations of the TDFP. It is found that the TDFP estimates obtained by the proposed method are similar to the reference values provided by MCS. These results confirm that the proposed EPAK method is capable of estimating the TDFP across varied subintervals with satisfactory accuracy. As shown in Fig. 5, the failure probability is rather low (e.g., around  $10^{-3}$ ) within small time intervals. The proposed method still maintains high estimation accuracy, which indicates the effectiveness of the proposed method in small TDFP problems.

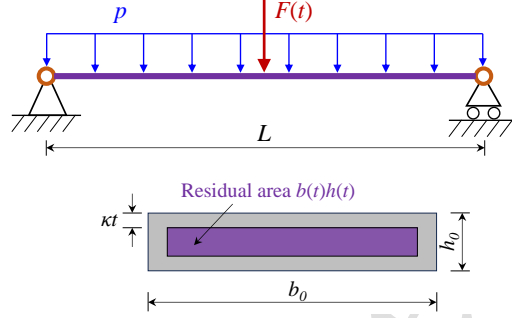


Figure 4: Schematic diagram of the corroded beam.

Table 2: Distributions of inputs of example 4.2.

Input variable	Distribution	Mean	Standard deviation	Autocorrelation function
$f_y$ (MPa)	Lognormal	240	24	-
$b_0$ (m)	Lognormal	0.2	0.01	-
$h_0$ (m)	Lognormal	0.03	0.003	-
$F(t)$ (kN)	Gaussian process	3.5	0.7	$\kappa(t_1, t_2) = \exp\left[-\frac{1}{25}(t_1 - t_2)^2\right]$

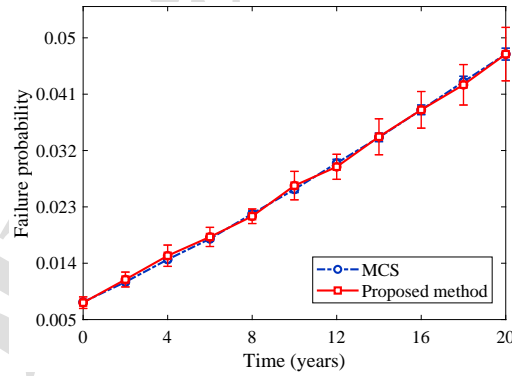


Figure 5: TDFP of example 4.2 ( $q = 1$ ).

Table 3: TRA results of example 4.2.

Methods	$N_{ite}$	$N_{eva}$	$\hat{P}_f$	$\epsilon_{\hat{P}_f}$	$COV[\hat{P}_f]$	CPU Time (s)
MCS	-	$201 \times 10^6$	$4.74 \times 10^{-2}$	-	0.45%	2.0
t-IRS <sup>1</sup>	-	171.4	$4.71 \times 10^{-2}$	0.63%	-	-
eSPT <sup>1</sup>	-	113.4	$4.88 \times 10^{-2}$	2.95%	-	-
STRA <sup>1</sup>	45.4	56.4	$4.78 \times 10^{-2}$	0.84%	-	-
SILK	40.4	51.4	$4.73 \times 10^{-2}$	0.21%	2.51%	432.8
REAL	31.1	42.1	$4.75 \times 10^{-2}$	0.21%	3.29%	183.9
Proposed method	$q = 1$	8.7	$4.78 \times 10^{-2}$	0.84%	4.50%	6.1
	$q = 2$	7.3	$4.74 \times 10^{-2}$	0	8.12%	7.2
	$q = 3$	6.1	$4.69 \times 10^{-2}$	1.05%	6.63%	6.8
	$q = 4$	4.9	$4.62 \times 10^{-2}$	2.53%	4.91%	6.5
	$q = 5$	4.2	$4.74 \times 10^{-2}$	0	3.98%	6.0
	$q = 6$	5.2	$4.79 \times 10^{-2}$	1.05%	3.14%	6.9
	$q = 7$	4.6	$4.76 \times 10^{-2}$	0.42%	5.85%	6.3
	$q = 8$	4.5	$4.60 \times 10^{-2}$	2.95%	3.51%	7.1

<sup>1</sup> The results are taken from research [60].

### 4.3. Turbine blade

A turbine blade model adapted from Matlab PDE toolbox is investigated as the third example, whose finite element model (FEM) and von Mises stress distribution are shown in Fig. 6. The Young's modulus, Poisson's ratio, coefficient of thermal expansion and the thermal conductivity are denoted as  $E$ ,  $\lambda$ ,  $\alpha$  and  $T_c$ , respectively. The temperature of the interior cooling air and the suction sides are denoted as  $T_1$  and  $T_2$ , respectively. In this example, failure is defined as the maximum von Mises stress exceeding an allowable threshold. Taking into account that the allowable threshold decreases with the time  $t$ , the LSF is defined as:

$$g(\mathbf{x}, \mathbf{F}(t), t) = \sigma_{at} e^{-0.02t} - \sigma_m(\mathbf{x}, \mathbf{F}(t)) \quad (46)$$

where  $\sigma_{at} = 1.5\text{GPa}$  represents the initial allowable threshold;  $\sigma_m(\mathbf{x}, \mathbf{F}(t))$  denotes the maximum stress provided by FEM;  $F_1(t)$  and  $F_2(t)$  in  $\mathbf{F}(t)$  represent the pressure loads at the pressure side and suction side, respectively. Table 4 lists the details of the input variables.

The time interval  $[0, 12]$  and the Gaussian processes  $F_1(t)$  and  $F_2(t)$  are discretized with 121 time instants, five and eight independent normal variables, respectively. Table 5 presents the TRA results using different methods. For MCS,  $121 \times 10^5$  LSF evaluations are required to ensure the accuracy of TDFP estimate, which is computationally prohibitive. Instead, a simplified simulation with 12,100 LSF evaluations (taking

approximately 3.76 hours) is performed to provide an approximate assessment of the computational time. The proposed method, SILK and REAL provide similar TDFP estimates, while the proposed method exhibits higher efficiency in terms of  $N_{ite}$  and computation time than the counterparts. When  $q$  varies from 1 to 8, the proposed method requires minimal  $N_{ite}$  for the setting of  $q = 5$ . As for the computation time, the setting of  $q = 4$  would minimize the computation time in this example.

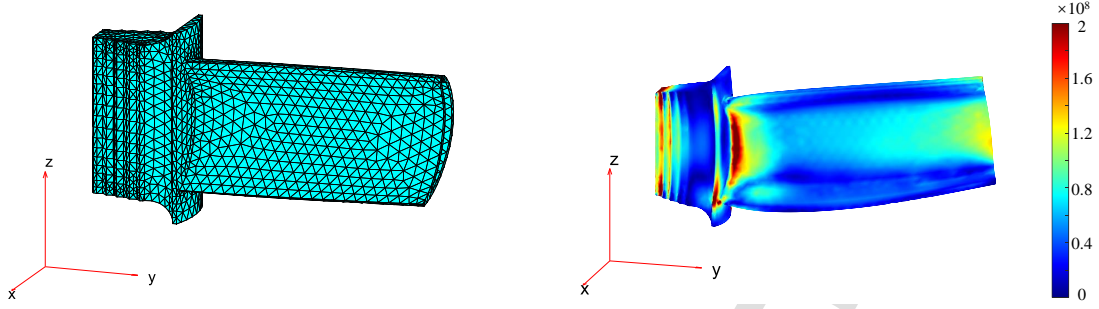


Figure 6: FEM and stress distribution of the turbine blade (unit: Pa).

Table 4: Distributions of inputs of example 4.3.

Variable	Distribution	Parameter 1	Parameter 2	Autocorrelation function
$E$	Normal	220	22	-
$\alpha$	Normal	$1.27 \times 10^{-5}$	$1.27 \times 10^{-6}$	-
$\lambda$	Lognormal	0.27	0.0216	-
$T_c$	Lognormal	11.5	1.38	-
$T_1$	Uniform	130	170	-
$T_2$	Uniform	950	1050	-
$F_1(t)$	Gaussian process	500	100	$\kappa(t_1, t_2) = \exp\left[-\frac{1}{16}(t_1 - t_2)^2\right]$
$F_2(t)$	Gaussian process	450	90	$\kappa(t_1, t_2) = \exp\left[-\frac{1}{4}(t_1 - t_2)^2\right]$

Note: For the uniform distributions, parameter 1 and 2 respectively represent the lower and upper bounds; for other distributions, they denote the mean and standard deviation, respectively.

#### 4.4. Arch bridge

In this section, a lower-bearing arch bridge with the calculated span of 150m and the rise-to-span ratio of 1:5 is considered [61], as shown in Fig. 7. The arch bridge features 34 suspenders, each spaced 6.8m apart. A three-dimensional FEM model is built on the OpenSEES platform, consisting of 241 nodes and 439 elements, as shown in Fig. 8. The elastic beam-column element is adopted to simulate the suspenders, main girder and arch ribs. A increasing heavy load  $F(t)$  applied in the mid-span is considered and modeled as a non-stationary Gaussian process. Considering that the suspenders are subjected to the corrosion effect,



Table 5: TRA results of example 4.3.

Methods	$N_{ite}$	$N_{eva}$	$\hat{P}_f$	$\epsilon_{\hat{P}_f}$	$COV[\hat{P}_f]$	CPU Time
MCS	-	$121 \times 10^5$	-	-	-	$\approx 157.0$ (days)
SILK	369.5	380.5	$5.28 \times 10^{-3}$	-	2.65%	29,962.6 (s)
REAL	191.3	202.3	$5.28 \times 10^{-3}$	0	6.86%	8382.3 (s)
Proposed method	$q = 1$	110.8	$5.19 \times 10^{-3}$	1.70%	5.41%	1121.4 (s)
	$q = 2$	58.7	$5.15 \times 10^{-3}$	2.46%	2.82%	1032.3 (s)
	$q = 3$	42.2	$5.36 \times 10^{-3}$	1.52%	4.49%	709.8 (s)
	$q = 4$	33.3	$5.33 \times 10^{-3}$	0.95%	6.08%	432.4 (s)
	$q = 5$	28.9	$5.28 \times 10^{-3}$	0	5.24%	643.2 (s)
	$q = 6$	36.4	$5.26 \times 10^{-3}$	0.38%	5.90%	769.4 (s)
	$q = 7$	34.7	$5.17 \times 10^{-3}$	2.08%	4.59%	858.8 (s)
	$q = 8$	37.9	$5.38 \times 10^{-3}$	1.89%	4.90%	1180.9 (s)

the residual area is denoted as  $A(t) = A_1 \times (1 - 0.007t)$ , where  $A_1$  is the initial area of the suspenders. The failure is defined as the maximum deflection in excess of a safety threshold  $\Delta_s = 10$  cm. The LSF is thus written as:

$$g(\mathbf{X}, F(t), t) = \Delta_s - \Delta(A(t), E_1, A_2, E_2, I, F_1, F(t)) \quad (47)$$

where the initial area of the arch ribs is denoted as  $A_2$ .  $E_1$  and  $E_2$  represent the Young's modulus for the suspenders and arch ribs, respectively; The main girder's stiffness is characterized by its area moment of inertia  $I$ ; The total applied load, including both dead and live components, is represented as  $F_1$ . Table 6 lists the details of input variables.

The time interval  $[0, 50]$  and the non-stationary Gaussian process  $F(t)$  are discretized with 501 time instants and sixteen independent normal variables, respectively. Fig. 9 shows one hundred realizations of  $F(t)$ . Table 7 presents the obtained TDFP estimates by different methods. Similar to the third example, the CPU time required by MCS is approximately calculated with 10,200 LSF evaluations in this example. The TDFP estimates obtained by all methods are relatively close; however, the proposed EPAK method demonstrates significantly higher efficiency than the other methods. Specifically, the proposed method with  $q = 1$  requires 66.6 LSF evaluations on average, while SILK and REAL requires 113.8 and 88.0 evaluations, respectively. Besides, the proposed method costs much less iterations than the counterparts when specifying a large value of  $q$ . As for the computation time, SILK and REAL takes 13,702.3 seconds and 6000.4 seconds, respectively, whereas the proposed EPAK method takes 270.1 to 456.2 seconds. When  $q$  varies from 1 to 8,

the required computation time is minimal for the setting of  $q = 5$ . Meanwhile, the corresponding  $N_{ite}$  and COV are relatively small.

The time-dependent reliability results are schematically depicted in Fig. 10, where the reliability index (denoted as  $\beta$ ) is obtained by  $\beta = \Phi^{-1}(1 - \hat{P}_f)$ . The error bars show the range of the mean  $\pm 2$  standard deviations of the TDFP and the reliability index, respectively. It can be observed that as the service life increases, the failure probability increases. Correspondingly, the reliability index gradually decreases, which following an approximately linear trend. Besides, the reliability index at  $t = 50$  ( $\beta_{50} = 2.95$ ) decreases by 29.76% compared to the initial service status ( $\beta_0 = 4.20$ ), which reflects the necessity of performing TRA for this arch bridge problem.

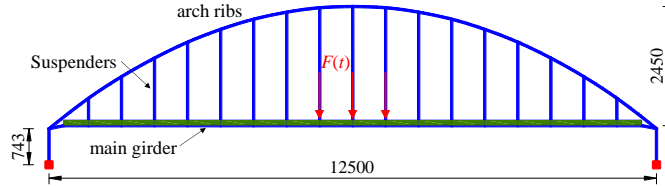


Figure 7: Illustrative diagram of the arch bridge (unit: cm).

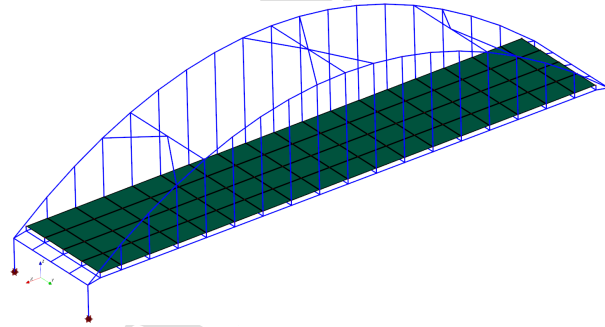


Figure 8: FEM of the arch bridge.

## 5. Conclusions

This study proposed a new method termed ‘Error-informed Parallel Adaptive Kriging’ (EPAK) for efficient TRA. Specifically, the VAIS was adapted in a sequential way to estimate the small TDFP based on the trained single-loop Kriging model, which could decrease the sample size and total computation

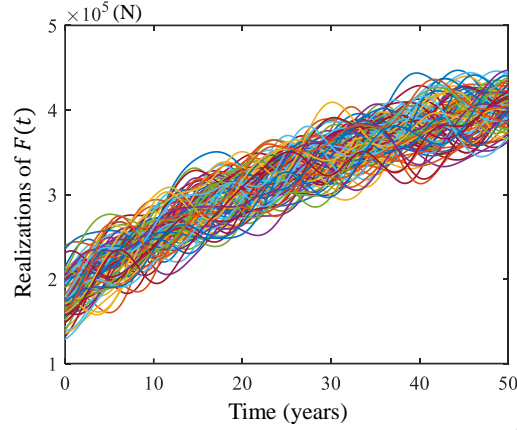


Figure 9: Realizations of the Gaussian process of example 4.4.

Table 6: Distributions of inputs of example 4.4.

Input variable	Distribution	Mean	Standard deviation	Autocorrelation function
$A_1(\text{m}^2)$	Lognormal	$3 \times 10^{-3}$	$3 \times 10^{-4}$	-
$E_1(\text{Pa})$	Normal	$2 \times 10^{11}$	$2 \times 10^{10}$	-
$A_2(\text{m}^2)$	Lognormal	2.8	0.28	-
$E_2(\text{Pa})$	Normal	$2.1 \times 10^{11}$	$2.1 \times 10^{10}$	-
$I(\text{m}^4)$	Lognormal	$5.6 \times 10^{-2}$	$8.4 \times 10^{-3}$	-
$F_1(\text{N/m})$	Gumbel	$5.5 \times 10^7$	$1.1 \times 10^7$	-
$F(t)(\text{kN})$	Gaussian process	$180 + 180 \ln \left(1 + \frac{t}{20}\right)$	$18 + 18 \ln \left(1 + \frac{t}{20}\right)$	$\kappa(t_1, t_2) = \exp \left[ -\frac{1}{16} (t_1 - t_2)^2 \right]$

time. Besides, the maximum relative error of TDFP estimation was derived, based on which a stopping criterion was developed by judging whether the maximum relative error was below a predefined threshold. Finally, a parallel sampling strategy was proposed through combining the relative error contribution and an introduced influence function, which could not only select multiple training points but also overcome the problem of unnecessary LSF evaluations caused by excessive clustering. Several examples were studied to validate the applicability of proposed EPAK method. Results demonstrated that the proposed method can estimate small TDFPs with satisfactory accuracy. More importantly, the proposed EPAK method required much less LSF evaluations, iterations and CPU time when compared to other TRA methods, demonstrating its superior efficiency. Besides, numerical results showed that selecting too many training points in each iteration did not necessarily result in a reduction in the number of iterations and the total computation time. According to the investigated examples, four or five points was sufficient and effective to select, and was therefore suggested for the proposed method.

Table 7: TRA results of example 4.4.

Methods	$N_{ite}$	$N_{eva}$	$\hat{P}_f$	$\epsilon_{\hat{P}_f}$	COV[ $\hat{P}_f$ ]	CPU Time	
MCS	-	$501 \times 10^6$	-	-	-	$\approx 6543.1$ (days)	
SILK	102.8	113.8	$1.57 \times 10^{-3}$	-	3.55%	13,702.2 (s)	
REAL	77.0	88.0	$1.60 \times 10^{-3}$	1.91%	4.29%	6000.4 (s)	
Proposed method	$q = 1$	55.6	66.6	$1.61 \times 10^{-3}$	2.55%	2.84%	456.2 (s)
	$q = 2$	29.4	68.8	$1.60 \times 10^{-3}$	1.91%	6.05%	282.3 (s)
	$q = 3$	22.3	75.9	$1.61 \times 10^{-3}$	2.55%	4.12%	279.0 (s)
	$q = 4$	17.0	76.0	$1.58 \times 10^{-3}$	0.64%	4.14%	354.9 (s)
	$q = 5$	15.3	83.5	$1.59 \times 10^{-3}$	1.27%	3.33%	270.1 (s)
	$q = 6$	15.8	100.8	$1.62 \times 10^{-3}$	3.18%	4.56%	355.8 (s)
	$q = 7$	15.2	111.4	$1.61 \times 10^{-3}$	2.55%	5.91%	389.1 (s)
	$q = 8$	13.8	114.4	$1.59 \times 10^{-3}$	1.27%	4.96%	340.0 (s)

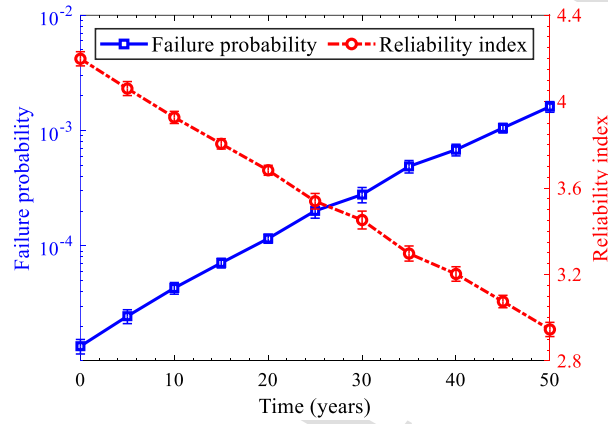


Figure 10: TDFP and reliability index of example 4.4.

The proposed EPAK method may perform weakly in high dimensions owing to the inherent limitations of the Kriging model. Further research is still required to address this problem. Besides, the proposed method could be adapted for time-dependent reliability-based design optimization.

#### Declaration of competing interest

The authors declare that they have no known competing financial interests or personal relationships that could have appeared to influence the work reported in this paper.

## Acknowledgments

This work was supported by the National Science Foundation for Distinguished Young Scholars of China (Grant No. 52425802), National Key Research and Development Program of China (Grant No. 2021YFB2600900) and Science and Technology Program of Hunan Provincial Department of Transportation (No.202309).

## Appendix A. Kriging model

Kriging model is an interpolation-based regression method including linear regression and stochastic process, which is written as [55]:

$$\hat{g}(\mathbf{x}) = \mathbf{f}^T(\mathbf{x})\boldsymbol{\zeta} + \epsilon(\mathbf{x}) \quad (\text{A.1})$$

where  $\hat{g}(\mathbf{x})$  denotes the predicted response;  $\mathbf{f}(\mathbf{x})$  is the basis function vector;  $\boldsymbol{\zeta}$  represents the regression coefficients vector;  $\epsilon(\mathbf{x})$  denotes a Gaussian process with the mean of zero and the covariance of  $\kappa(\mathbf{x}^{(i)}, \mathbf{x}^{(j)}) = \sigma^2 R(\mathbf{x}^{(i)}, \mathbf{x}^{(j)})$ , where  $R(\mathbf{x}^{(i)}, \mathbf{x}^{(j)})$  is the correlation function and denoted as:

$$R(\mathbf{x}^{(i)}, \mathbf{x}^{(j)}) = \exp \left[ - \sum_{k=1}^n \theta_k \left( x_k^{(i)} - x_k^{(j)} \right)^2 \right] \quad (\text{A.2})$$

where  $\theta_k$  ( $k = 1, 2, \dots, n$ ) are correlation parameters and estimated using the maximum likelihood method [55]. Given  $n_0$  training points  $\mathbf{X} = [\mathbf{x}^{(1)}, \mathbf{x}^{(2)}, \dots, \mathbf{x}^{(n_0)}]$  and the responses  $\mathbf{G} = [g(\mathbf{x}^{(1)}), g(\mathbf{x}^{(2)}), \dots, g(\mathbf{x}^{(n_0)})]$ ,  $\boldsymbol{\zeta}$  and  $\sigma^2$  are estimated as:

$$\hat{\boldsymbol{\zeta}} = (\mathbf{F}^T \mathbf{R}^{-1} \mathbf{F})^{-1} \mathbf{F}^T \mathbf{R}^{-1} \mathbf{G} \quad (\text{A.3})$$

$$\hat{\sigma}^2 = \frac{(\mathbf{G} - \hat{\boldsymbol{\zeta}})^T \mathbf{R}^{-1} (\mathbf{G} - \hat{\boldsymbol{\zeta}} \mathbf{F})}{n_0} \quad (\text{A.4})$$

where  $\mathbf{F}$  is the regression matrix with  $F_{i,j} = f_j(\mathbf{x}^{(i)})$ ,  $i = 1, \dots, n_0$ ,  $j = 1, \dots, n$ ;  $\mathbf{R} = [R(\mathbf{x}^{(i)}, \mathbf{x}^{(j)})]$  ( $i, j = 1, \dots, n_0$ ) is the correlation matrix.

The mean prediction  $\mu_{\hat{g}}(\mathbf{x})$  and the variance prediction  $\sigma_{\hat{g}}^2(\mathbf{x})$  are obtained as follows:

$$\mu_{\hat{g}}(\mathbf{x}) = \mathbf{f}^T(\mathbf{x})\hat{\boldsymbol{\zeta}} + \mathbf{r}^T(\mathbf{x})\mathbf{R}^{-1}(\mathbf{G} - \mathbf{F}\hat{\boldsymbol{\zeta}}) \quad (\text{A.5})$$

$$\sigma_{\hat{g}}^2(\mathbf{x}) = \hat{\sigma}^2 \left[ 1 + \mathbf{u}^T(\mathbf{x}) (\mathbf{F}^T \mathbf{R}^{-1} \mathbf{F})^{-1} \mathbf{u}(\mathbf{x}) - \mathbf{r}^T(\mathbf{x}) \mathbf{R}^{-1} \mathbf{r}(\mathbf{x}) \right] \quad (\text{A.6})$$

where  $\mathbf{u}(\mathbf{x}) = \mathbf{F}^T \mathbf{R}^{-1} \mathbf{r}(\mathbf{x}) - \mathbf{f}(\mathbf{x})$ ;  $\mathbf{r}(\mathbf{x}) = [R(\mathbf{x}, \mathbf{x}^{(1)}), \dots, R(\mathbf{x}, \mathbf{x}^{(n_0)})]^T$  is the correlation coefficient vector between the predicted point and the training set. Note that the construction and prediction of the Kriging model can be easily performed with DACE toolbox. More details may refer to [62].

## References

- [1] P. Gardoni, Risk and reliability analysis, Springer, 2017.
- [2] H. Guo, J. Zhang, Y. Dong, D. M. Frangopol, Probability-informed neural network-driven point-evolution kernel density estimation for time-dependent reliability analysis, Reliability Engineering & System Safety 249 (2024) 110234.
- [3] S. Li, X. Wang, R. Pang, B. Xu, A novel method for time-dependent small failure probability estimation of slope instability subjected to stochastic seismic excitations, Reliability Engineering & System Safety (2025) 111032.
- [4] B. Zhang, W. Wang, Y. Wang, Y. Li, C.-Q. Li, A critical review on methods for time-dependent structural reliability, Sustainable and Resilient Infrastructure 9 (2) (2024) 91–106.
- [5] C. Wang, M. Beer, B. M. Ayyub, Time-dependent reliability of aging structures: Overview of assessment methods, ASCE-ASME Journal of Risk and Uncertainty in Engineering Systems, Part A: Civil Engineering 7 (4) (2021) 03121003.
- [6] D. Wang, H. Qiu, L. Gao, C. Jiang, A Subdomain uncertainty-guided Kriging method with optimized feasibility metric for time-dependent reliability analysis, Reliability Engineering & System Safety 243 (2024) 109839.
- [7] S. O. Rice, Mathematical analysis of random noise, The Bell System Technical Journal 23 (3) (1944) 282–332.
- [8] C. Andrieu-Renaud, B. Sudret, M. Lemaire, The PHI2 method: a way to compute time-variant reliability, Reliability Engineering & System Safety 84 (1) (2004) 75–86.
- [9] B. Sudret, Analytical derivation of the outcrossing rate in time-variant reliability problems, Structure and Infrastructure Engineering 4 (5) (2008) 353–362.
- [10] X.-Y. Zhang, Z.-H. Lu, S.-Y. Wu, Y.-G. Zhao, An efficient method for time-variant reliability including finite element analysis, Reliability Engineering & System Safety 210 (2021) 107534.
- [11] B. Zhang, W. Wang, H. Lei, X. Hu, C.-Q. Li, An improved analytical solution to outcrossing rate for scalar nonstationary and non-gaussian processes, Reliability Engineering & System Safety 247 (2024) 110102.

- [12] W. Yang, B. Zhang, W. Wang, C.-Q. Li, Time-dependent structural reliability under nonstationary and non-gaussian processes, *Structural Safety* 100 (2023) 102286.
- [13] X.-W. Li, X.-Y. Zhang, Y.-G. Zhao, Outcrossing rate method for nonstationary non-Gaussian performance functions and its application to time-dependent reliability assessment, *Journal of Engineering Mechanics* 150 (10) (2024) 04024078.
- [14] Z. Hu, X. Du, Time-dependent reliability analysis with joint upcrossing rates, *Structural and Multidisciplinary Optimization* 48 (2013) 893–907.
- [15] C. Wang, Stochastic process-based structural reliability considering correlation between upcrossings, *ASCE-ASME Journal of Risk and Uncertainty in Engineering Systems, Part A: Civil Engineering* 6 (4) (2020) 06020002.
- [16] Z. P. Mourelatos, M. Majcher, V. Pandey, I. Baseski, Time-dependent reliability analysis using the total probability theorem, *Journal of Mechanical Design* 137 (3) (2015) 031405.
- [17] C. Jiang, X. Huang, X. Han, D. Zhang, A time-variant reliability analysis method based on stochastic process discretization, *Journal of Mechanical Design* 136 (9) (2014) 091009.
- [18] C. Gong, D. M. Frangopol, An efficient time-dependent reliability method, *Structural Safety* 81 (2019) 101864.
- [19] Z. Hu, X. Du, First order reliability method for time-variant problems using series expansions, *Structural and Multidisciplinary Optimization* 51 (2015) 1–21.
- [20] H. Li, T. Wang, J. Yuan, H. Zhang, A sampling-based method for high-dimensional time-variant reliability analysis, *Mechanical Systems and Signal Processing* 126 (2019) 505–520.
- [21] X. Yuan, W. Zheng, C. Zhao, M. A. Valdebenito, M. G. Faes, Y. Dong, Line sampling for time-variant failure probability estimation using an adaptive combination approach, *Reliability Engineering & System Safety* 243 (2024) 109885.
- [22] X. Yuan, Y. Shu, Y. Qian, Y. Dong, Adaptive importance sampling approach for structural time-variant reliability analysis, *Structural Safety* (2024) 102500.
- [23] Y. Zhang, J. Xu, M. Beer, A single-loop time-variant reliability evaluation via a decoupling strategy and probability distribution reconstruction, *Reliability Engineering & System Safety* 232 (2023) 109031.
- [24] Y. Zhang, J. Xu, P. Gardoni, A loading contribution degree analysis-based strategy for time-variant reliability analysis of structures under multiple loading stochastic processes, *Reliability Engineering & System Safety* 243 (2024) 109833.
- [25] L. Ouyang, Y. Che, C. Park, Y. Chen, A novel active learning Gaussian process modeling-based method for time-dependent reliability analysis considering mixed variables, *Reliability Engineering & System Safety* 244 (2024) 109916.
- [26] P. Hao, H. Tian, H. Yang, Y. Zhang, S. Feng, An efficient sequential Kriging model for structure safety lifetime analysis considering uncertain degradation, *Reliability Engineering & System Safety* 255 (2025) 110669.
- [27] H. Zhan, N.-C. Xiao, A new active learning surrogate model for time-and space-dependent system reliability analysis, *Reliability Engineering & System Safety* 253 (2025) 110536.
- [28] Z. Wang, P. Wang, A nested extreme response surface approach for time-dependent reliability-based design optimization, *Journal of Mechanical Design* 134 (12) (2012) 121007.

- [29] J. Wu, Z. Jiang, H. Song, L. Wan, F. Huang, Parallel efficient global optimization method: a novel approach for time-dependent reliability analysis and applications, *Expert Systems with Applications* 184 (2021) 115494.
- [30] Z. Wang, W. Chen, Confidence-based adaptive extreme response surface for time-variant reliability analysis under random excitation, *Structural Safety* 64 (2017) 76–86.
- [31] H. Li, Z. Lu, K. Feng, A double-loop Kriging model algorithm combined with importance sampling for time-dependent reliability analysis, *Engineering with Computers* 40 (3) (2024) 1539–1558.
- [32] Z. Hu, X. Du, Mixed efficient global optimization for time-dependent reliability analysis, *Journal of Mechanical Design* 137 (5) (2015) 051401.
- [33] Z. Hu, S. Mahadevan, A single-loop kriging surrogate modeling for time-dependent reliability analysis, *Journal of Mechanical Design* 138 (6) (2016) 061406.
- [34] C. Zha, C. Pan, Z. Sun, Q. Liu, A single-loop reliability sensitivity analysis strategy for time-dependent rare events with both random variables and stochastic processes, *Reliability Engineering & System Safety* 251 (2024) 110373.
- [35] Z. Song, H. Zhang, L. Zhang, Z. Liu, P. Zhu, An estimation variance reduction-guided adaptive Kriging method for efficient time-variant structural reliability analysis, *Mechanical Systems and Signal Processing* 178 (2022) 109322.
- [36] C. Jiang, H. Qiu, L. Gao, D. Wang, Z. Yang, L. Chen, Real-time estimation error-guided active learning Kriging method for time-dependent reliability analysis, *Applied Mathematical Modelling* 77 (2020) 82–98.
- [37] C. Dang, M. A. Valdebenito, M. G. Faes, Towards a single-loop Gaussian process regression based-active learning method for time-dependent reliability analysis, *Mechanical Systems and Signal Processing* 226 (2025) 112294.
- [38] H.-M. Qian, H.-Z. Huang, Y.-F. Li, A novel single-loop procedure for time-variant reliability analysis based on Kriging model, *Applied Mathematical Modelling* 75 (2019) 735–748.
- [39] C. Jiang, D. Wang, H. Qiu, L. Gao, L. Chen, Z. Yang, An active failure-pursuing Kriging modeling method for time-dependent reliability analysis, *Mechanical Systems and Signal Processing* 129 (2019) 112–129.
- [40] R. Cao, Z. Sun, J. Wang, F. Guo, A single-loop reliability analysis strategy for time-dependent problems with small failure probability, *Reliability Engineering & System Safety* 219 (2022) 108230.
- [41] W. Yun, Z. Lu, L. Wang, A coupled adaptive radial-based importance sampling and single-loop Kriging surrogate model for time-dependent reliability analysis, *Structural and Multidisciplinary Optimization* 65 (5) (2022) 139.
- [42] F. Xin, P. Wang, Y. Chen, R. Yang, F. Hong, A new uncertainty reduction-guided single-loop Kriging coupled with subset simulation for time-dependent reliability analysis, *Reliability Engineering & System Safety* (2025) 111065.
- [43] F. Hong, P. Wei, J. Fu, Y. Xu, W. Gao, A new acquisition function combined with subset simulation for active learning of small and time-dependent failure probability, *Structural and Multidisciplinary Optimization* 66 (4) (2023) 72.
- [44] H. Guo, Y. Dong, P. Gardoni, Adaptive subset simulation for time-dependent small failure probability incorporating first failure time and single-loop surrogate model, *Structural Safety* 102 (2023) 102327.
- [45] D. Wang, H. Qiu, L. Gao, C. Jiang, A single-loop Kriging coupled with subset simulation for time-dependent reliability



- analysis, Reliability Engineering & System Safety 216 (2021) 107931.
- [46] Z. Hu, D. Wang, C. Dang, M. Beer, L. Wang, Uncertainty-aware adaptive Bayesian inference method for structural time-dependent reliability analysis, Submitted to Reliability Engineering & System Safety (2024).
- [47] C. Dang, P. Wei, J. Song, M. Beer, Estimation of failure probability function under imprecise probabilities by active learning-augmented probabilistic integration, ASCE-ASME Journal of Risk and Uncertainty in Engineering Systems, Part A: Civil Engineering 7 (4) (2021) 04021054.
- [48] C. Dang, M. A. Valdebenito, M. G. Faes, P. Wei, M. Beer, Structural reliability analysis: A Bayesian perspective, Structural Safety 99 (2022) 102259.
- [49] L. Wang, Z. Hu, C. Dang, M. Beer, Refined parallel adaptive Bayesian quadrature for estimating small failure probabilities, Reliability Engineering & System Safety 244 (2024) 109953.
- [50] C.-C. Li, A. Der Kiureghian, Optimal discretization of random fields, Journal of Engineering Mechanics 119 (6) (1993) 1136–1154.
- [51] K.-K. Phoon, H. Huang, S. T. Quek, Simulation of strongly non-Gaussian processes using Karhunen–Loeve expansion, Probabilistic Engineering Mechanics 20 (2) (2005) 188–198.
- [52] G. Deodatis, M. Shields, The spectral representation method: A framework for simulation of stochastic processes, fields, and waves, Reliability Engineering & System Safety (2024) 110522.
- [53] Z. Wang, A. Shafieezadeh, ESC: an efficient error-based stopping criterion for kriging-based reliability analysis methods, Structural and Multidisciplinary Optimization 59 (2019) 1621–1637.
- [54] D. Zhan, J. Qian, Y. Cheng, Pseudo expected improvement criterion for parallel EGO algorithm, Journal of Global Optimization 68 (2017) 641–662.
- [55] B. Echard, N. Gayton, M. Lemaire, AK-MCS: An active learning reliability method combining Kriging and Monte Carlo Simulation, Structural Safety 33 (2) (2011) 145–154.
- [56] C. Dang, M. Beer, Semi-Bayesian active learning quadrature for estimating extremely low failure probabilities, Reliability Engineering & System Safety 246 (2024) 110052.
- [57] Z. Zhao, Z.-H. Lu, Y.-G. Zhao, P-AK-MCS: Parallel AK-MCS method for structural reliability analysis, Probabilistic Engineering Mechanics 75 (2024) 103573.
- [58] H. Zhan, H. Liu, N.-C. Xiao, Time-dependent reliability analysis of structural systems based on parallel active learning Kriging model, Expert Systems with Applications 247 (2024) 123252.
- [59] Z. Wang, W. Chen, Time-variant reliability assessment through equivalent stochastic process transformation, Reliability Engineering & System Safety 152 (2016) 166–175.
- [60] W. Hu, J. Yan, F. Zhao, C. Jiang, H. Liu, H. Cho, I. Lee, Surrogate-based time-dependent reliability analysis for a digital twin, Journal of Mechanical Design 145 (9) (2023).
- [61] X. Chen, Z. Lin, Structural nonlinear analysis program OpenSEES theory and tutorial, China Architecture & Building

577 Press: Beijing, China (2014) 87–89.

578 [62] S. N. Lophaven, H. B. Nielsen, J. Sondergaard, DACE: A Matlab Kriging toolbox, Technical University of Denmark,  
579 Kongens Lyngby, Technical Report No. IMM-TR-2002-12 (2002).

### Highlights

- Error-informed parallel adaptive Kriging is proposed for time-dependent reliability analysis
- A sequential variance amplified importance sampling technique is developed
- The maximum relative error of time-dependent failure probability is derived
- A parallel sampling strategy is proposed to enable parallel computing
- The superior efficiency and accuracy of the proposed method is verified

## Conflict of Interest

There are no conflicts of interest.

**Declaration of interests**

☒ The authors declare that they have no known competing financial interests or personal relationships that could have appeared to influence the work reported in this paper.

☐ The authors declare the following financial interests/personal relationships which may be considered as potential competing interests: